ARTICLES
PUBLISHED ONLINE: 4 SEPTEMBER 2011 | DOI: 10.1038/NNANO.2011.147
nature nanotechnology

Nanopore-based detection of circulating microRNAs in lung cancer patients

Yong Wang[1†], Dali Zheng[2†], Qiulin Tan[1], Michael X. Wang[2*] and Li-Qun Gu[1*]

MicroRNAs are short RNA molecules that regulate gene expression, and have been investigated as potential biomarkers because their expression levels are correlated with various diseases. However, detecting microRNAs in the bloodstream remains difficult because current methods are not sufficiently selective or sensitive. Here, we show that a nanopore sensor based on the α-haemolysin protein can selectively detect microRNAs at the single molecular level in plasma samples from lung cancer patients without the need for labels or amplification of the microRNA. The sensor, which uses a programmable oligonucleotide probe to generate a target-specific signature signal, can quantify subpicomolar levels of cancer-associated microRNAs and can distinguish single-nucleotide differences between microRNA family members. This approach is potentially useful for quantitative microRNA detection, the discovery of disease markers and non-invasive early diagnosis of cancer.

MicroRNAs are a class of short (~18–22 nucleotides) non-coding RNAs that are important in development and cell differentiation, the regulation of the cell cycle, apoptosis and signalling pathways[1,2]. Since its initial discovery in *Caenorhabditis elegans* in 1993 (ref. 3), over 17,000 microRNAs have been identified across different species, including humans[4]. In the cytoplasm, mature microRNAs are associated with an RNA-induced silencing protein complex to bind with the 3′-untranslated region of target messenger RNAs[1,5,6]. By either repressing translation or cleaving the target messenger RNA[1,5,6], these microRNAs regulate around 30% of human gene expression[5] at the post-transcriptional level. Aberrant expression of microRNAs has been found in all types of tumours[7,8], and different types of cancers have distinct microRNA profiles[9]. Interestingly, microRNAs can be released from the primary tumour into the bloodstream in a stable form[10]. Circulating microRNAs are enveloped inside exosomal vesicles and are transferable to and functional in recipient cells[11–13]. Therefore, the detection of tumour-specific circulating microRNAs is useful for the early diagnosis, staging and monitoring of cancer[7,8,10–13].

Quantitative reverse transcription real-time polymerase chain reaction (qRT-PCR) assays and microarrays have been developed for the detection of microRNA. However, these methods suffer from error-prone amplification, cross-hybridization, and a lack of valid internal controls[14,15] because the shortness of the microRNA sequences makes it difficult to design probes and primers. Other techniques based on colorimetry, bioluminescence, enzyme turnover and electrochemistry have been proposed, and nanoparticles, molecular beacons, deep sequencing[16,17] and single-molecule fluorescence[18] have also been applied to microRNA detection (for reviews, see refs 16, 17). However, many of these methods still require the labelling and chemical modification of the target or expensive instruments.

The nanopore is a molecular-scale pore structure that is able to detect, with high sensitivity, the position and conformation of a single molecule that is present within the pore lumen[19]. From the characteristic change in nanopore conductance, one can electrically elucidate single-molecule kinetic pathways and quantify the target. Various nanopore sensors are being developed with broad biotechnological applications[19–24] (for reviews, see refs 19–23), including the next generation of DNA sequencing technology[25,26]. The development of nanopore-based microRNA detectors is a novel effort in this rapidly evolving field, and Wanunu *et al.* first reported the use of a 3 nm synthetic pore to quantify the translocation of enriched microRNAs that were hybridized to a probe[27]. In this report, we construct a protein-nanopore-based sensor that enables sensitive, selective and direct quantification of cancer-associated microRNAs in the blood and discrimination of single-nucleotide differences in microRNA family members.

Generation of microRNA signatures in the nanopore

We used the α-haemolysin protein pore, a toxin from *Staphylococcus aureus* bacterium[28], as the sensor element. The translocation of single-stranded oligonucleotides through this 2 nm pore has been studied extensively[29–32]. However, it is difficult to distinguish the translocation of different microRNAs because the sequences of all microRNAs are short and similar in length. One way of overcoming this challenge is to use a signature that can detect target microRNA in the mixture. We identified such a microRNA signature signal in the nanopore using an oligonucleotide probe.

The probe structure is shown in Fig. 1a. The capture domain of the probe was used to bind the target microRNA by Watson–Crick base pairing in the solution. Each end (3′ and 5′) of the capture domain was extended with a poly(dC)$_{30}$ signal tag. Our first target was miR-155, a lung-cancer-associated microRNA[12,13,33]. Figure 1b illustrates a sequence of nanopore current events in the presence of miR-155 and its probe, P_{155}, on the *cis* side of the pore. The boxed events represent a characteristic type of multi-level block that was generated by the miR-155·P_{155} hybrid. This block type was not observed in the presence of miR-155 or P_{155} alone in the *cis* solution. In a multi-level block (Fig. 1c, left panel), the Level 1 state lasted for 250 ± 58 ms, which is almost equal to the entire event duration, and significantly reduced the nanopore current, with a relative residual conductance (g/g_0) of 0.15. The Level 1 state was followed

[1]Department of Biological Engineering and Dalton Cardiovascular Research Center, University of Missouri, Columbia, MO 65211, [2]Ellis Fischel Cancer Center and Department of Pathology and Anatomical Sciences, University of Missouri, Columbia, MO 65211, USA; †These authors contributed equally to this work.
*e-mail: gul@missouri.edu; wangmx@health.missouri.edu

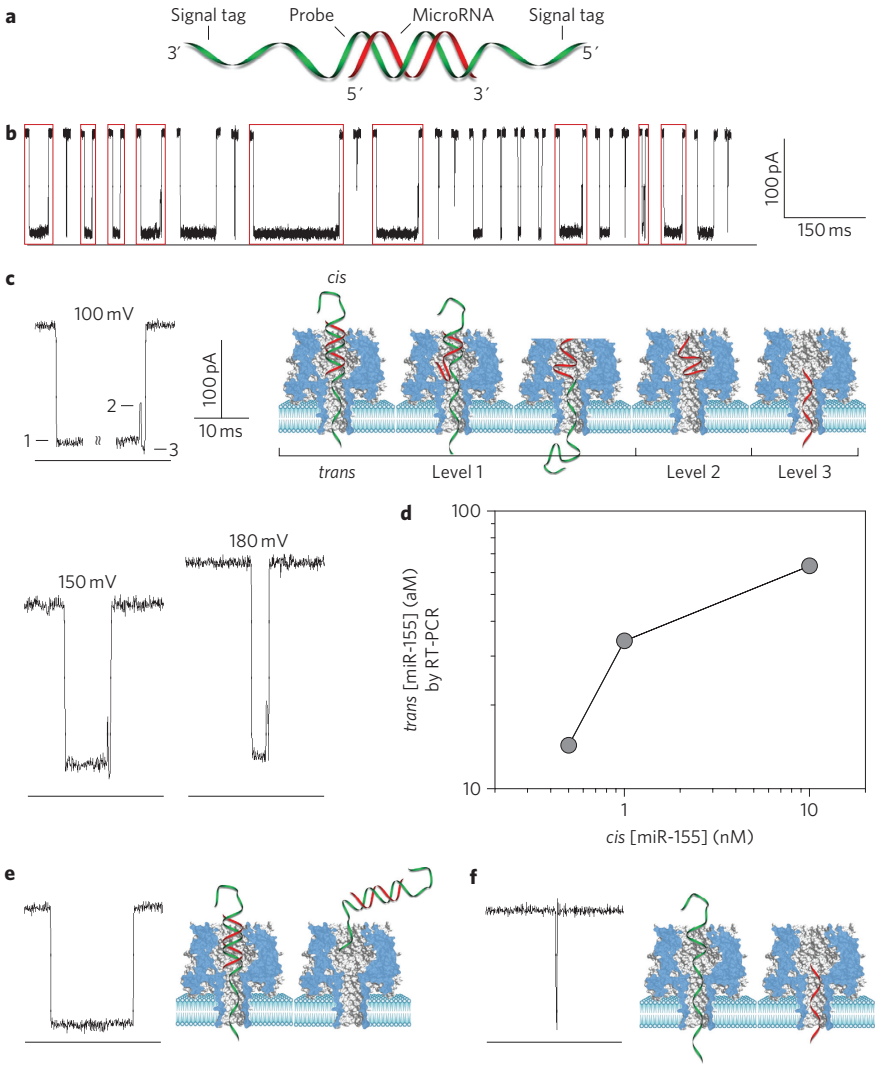

Figure 1 | Capturing single microRNA molecules in the nanopore. a, Molecular diagram of a microRNA (red) bound to a probe (green) bearing signal tags on each end. **b**, Sequence of nanopore current blocks in the presence of 100 nM miR-155 and 100 nM P_{155} in the *cis* solution. Traces were recorded at +100 mV in solutions containing 1 M KCl buffered with 10 mM Tris (pH 8.0). Red boxes represent the multi-level current pattern. **c**, A typical multi-level long block (from **b**) at +100 mV generated by the miR-155·P_{155} hybrid. Right panel: diagram showing the molecular mechanism of hybrid dissociation and translocation. Level 1: trapping of the microRNA·probe hybrid in the pore, unzipping of the microRNA from the probe and translocation of the probe through the pore. Level 2: unzipped microRNA residing in the pore cavity. Level 3: translocation of the unzipped microRNA through the pore. Lower panel: multi-level blocks at +150 and +180 mV. Increasing the voltage reduced the duration of Levels 1 and 3, which supports the above mechanistic model. **d**, miR-155 levels detected by qRT-PCR in *trans* solutions. Before detection, the pore current was monitored in 0.5 M/3 M (*cis*/*trans*) KCl at +180 mV in the presence of 1 μM P_{155} and 0.5, 1 or 10 nM of miR-155 in the *cis* solution. A much higher probe concentration than microRNA was used to enhance their hybridization in the *cis* solution (see Supplementary Information S1). **e**, A single-level block (from **b**) generated by a trapped miR-155·P_{155} hybrid that exited the pore from the *cis* entrance without unzipping and translocation. **f**, A spike-like short block generated by the translocation of unhybridized miR-155 or P_{155} from the *cis* solution.

by a discrete current increase to the Level 2 state, which persisted for 410 ± 20 μs, with a g/g_0 of 0.42. Finally, the current dropped to the Level 3 state and remained there for 270 ± 30 μs before returning to the full open base level. Similar to Level 1, Level 3 almost fully reduced the pore current, with a g/g_0 of 0.08. The right panel in Fig. 1c depicts the molecular configurations that correspond to the multi-level block. The amplitude and duration of Level 1 were consistent with a configuration in which the miR-155·P_{155} complex was trapped in the nanopore at the 2.6 nm *cis* opening, with either the 3′ or 5′ signal tag of P_{155} occupying the 1.6–2.0 nm β-barrel. Driven by the transmembrane voltage, the signal tag in the β-barrel induced the dissociation of miR-155·P_{155}. The dissociation time (the duration of Level 1) was comparable to previously reported timescales for DNA unzipping in the pore[34,35]. After unzipping, P_{155} left the pore through the narrower (*trans*) opening, and the Level 1 state was terminated. The Level 2 state featured large residue conductance, which should correspond to a configuration in which mir-155 unzipped from miR-155·P_{155} and temporarily resided in the nanocavity. This result is consistent with a previous finding which showed that an oligonucleotide trapped in the nanocavity can generate partial blocks[36]. The miR-155 in the nanocavity finally passed through the β-barrel to yield the short-lived Level 3 state. The duration of Level 3 (270 μs) was consistent with the translocation duration of miR-155 alone (220 μs) and the timescale for DNA or RNA translocations in previous studies[29–32]. The molecular mechanism described above was further proved by the voltage-dependent durations of Levels 1 and 3. Level 1 was shortened by a factor of 23 to 11 ms and Level 3 by a factor of 2 to 150 μs as the voltage increased from +100 to +180 mV (Fig. 1c, lower panel). This indicated that the voltage both enhanced the unzipping of miR-155·P_{155} and

accelerated the translocation of miR-155 (ref. 30). After the electrical recording, we quantified miR-155 in the *trans* solution using qRT-PCR (Fig. 1d and Supplementary Information S1). For 0.5, 1 and 10 nM of *cis* miR-155 (1 μM of P_{155}), the corresponding *trans* miR-155 concentration values were 14, 34 and 63 aM. The *trans* miR-155 identification verifies that the microRNA that unzipped from the microRNA·probe hybrid indeed translocated to the *trans* side of the pore.

The miR-155·P_{155} hybrid also produced single-level long blocks that had the same conductance ($g/g_0 = 0.15$) as Level 1 of the multi-level block (Fig. 1e). The single-level block was formed by the trapped miR-155·P_{155} complex that returned to the *cis* solution without unzipping and translocation. The frequency ratio of multi-level to single-level events monotonically increased with voltage, from 0.42 at +100 mV to 1.4 at +180 mV (Supplementary Table S2). This voltage-dependent frequency variation was consistent with the expectation that higher voltage increases the unzipping probability of miR-155·P_{155} and decreases its probability of escaping. In addition to the characteristic long events, we observed spike-like short blocks in the same recordings (Fig. 1f). Both their duration (220 ± 21 μs) and conductance ($g/g_0 = 0.16$) were similar to the translocation of unhybridized miR-155 or P_{155} present in the *cis* solution (Supplementary Fig. S1).

The above analysis indicates two important functions performed by the signal tag of the probe: guidance of the microRNA·probe complex entrapment in the pore and inducement of the dissociation of the microRNA·probe complex. The configuration change during the unzipping process gave rise to signature current patterns, which enabled the recognition of single target microRNA molecules. Because of the specificity of the probe, the frequency of the signature signal (f_{sig}) was independent of the presence of multiple nucleic acid components (Supplementary Fig. S3) and could therefore be used to quantify target microRNA in the mixture. Overall, the signature signal ensured the high selectivity required for microRNA detection in plasma RNA extract.

Quantification of microRNAs using optimized probes

The frequency of signature events can be used to quantify microRNA by the equation $f_{sig} = k_{on}[miR]_0$, where $[miR]_0$ is microRNA concentration and k_{on} is the occurrence rate constant of signature events (Supplementary Information S2). k_{on} is a key parameter that quantifies sensitivity and can be greatly improved by optimization of the probe structure. The left panel of Fig. 2a shows the traces for detecting miR-155 using probes with a poly(dC)$_{30}$ tag at the 5′ end ($P_{5'\text{-}C30}$), 3′ end ($P_{3'\text{-}C30}$) or both ends (P_{155}). The right panel compares the k_{on} values for different probes. The probe without the signal tag (P_{nt}) gave the lowest k_{on} at $2.8 \pm 0.6 \times 10^4\ M^{-1}\ s^{-1}$. k_{on} tripled to $6.8 \pm 1.3 \times 10^4\ M^{-1}\ s^{-1}$ when the probe was attached to a poly(dC)$_{30}$ tag at the 5′ end ($P_{5'\text{-}C30}$). However, k_{on} increased by a factor of 50 to $1.4 \pm 0.3 \times 10^6\ M^{-1}\ s^{-1}$ when the poly(dC)$_{30}$ tag was attached to the 3′ end ($P_{3'\text{-}C30}$). This orientation discrimination of single-stranded oligonucleotides in the nanopore is consistent with previous studies[37,38]. As expected, the P_{155} probe that contained both 3′ and 5′ poly(dC)$_{30}$ achieved the highest k_{on} at $2.0 \pm 0.2 \times 10^6\ M^{-1}\ s^{-1}$. In addition to tag directionality, k_{on} also depends on tag length. For example, the poly(dC)$_{30}$ tag showed higher efficiency in the generation of signature events than a shorter tag, such as poly(dC)$_8$, and was more efficient than the poly(dA)$_{30}$ and poly(dT)$_{30}$ tags (unpublished data).

Using P_{155} as the probe, we verified that the frequency of the signature event was proportional to the miR-155 concentration range from 10 to 100 nM (Fig. 2b, left panel). This correlation was measured at +100 mV in 1 M KCl. The frequencies in any two miR-155 concentrations, such as 10 and 25 nM, were significantly separated ($P < 0.005$). Wanunu *et al.* reported that a gradient of salt concentration across a synthetic nanopore greatly increases

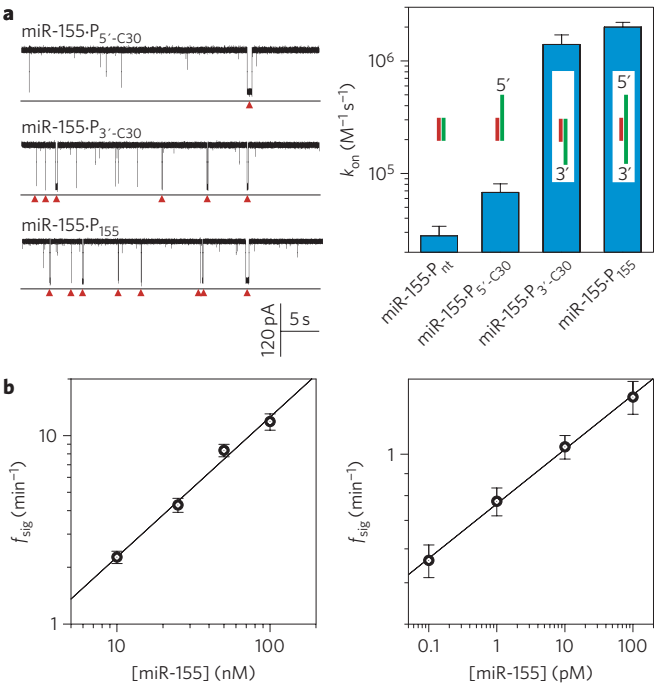

Figure 2 | Optimizing the probe sequence for enhanced detection sensitivity. a, Left panel: current traces showing the frequencies of signature events for miR-155 hybridized to the probes $P_{5'\text{-}C30}$ (top), $P_{3'\text{-}C30}$ (middle) and P_{155} (bottom), monitored at +100 mV in 1 M KCl. Right panel: occurrence rate constant of signature events for miR-155 detection with different probes (see Supplementary Table S3 for details). **b**, Left panel: [miR-155]—f_{155} correlation for target concentration ranges between 10 and 100 nM in 1 M KCl. Right panel: [miR-155]—f_{155} correlation measured in 0.2 M/3 M (*cis*/*trans*) KCl with much lower target concentrations (between 0.1 and 100 pM). Data in both panels were measured at +100 mV. The results between any two miR-155 concentrations were statistically significant ($P < 0.01$).

the capture rate of dsDNA[39]. Similarly, the use of asymmetrical KCl solutions (0.2 M/3 M, *cis*/*trans*) allowed measurement of the frequency of microRNA events at far lower concentrations, from 0.1 to 100 pM (Fig. 2b, right panel). In addition to the use of asymmetric solutions, the application of high voltage (Supplementary Fig. S2) and the use of an engineered nanopore[40] also proved effective in increasing the event frequency for high sensitivity.

Discrimination of microRNAs with similar sequences

Among the over 1,400 human microRNAs that have been identified, many members of the same microRNA family have similar sequences or single-nucleotide polymorphisms (SNPs)[4]. The SNPs are associated with significant biological properties of cancers, such as susceptibility, prognosis and response to therapeutic agents[41]. However, sequence-similar microRNAs or SNPs are difficult to distinguish using current PCR or hybridization-based methods[14–16]. Because dsDNAs that contain a single-nucleotide mismatch are identifiable in the nanopore based on their unzipping times[35,42–44], we decided to study whether the nanopore could distinguish single-nucleotide differences in microRNA family members.

We selected the *let-7* tumour-suppressing microRNA family[7–9] as the target. *Let-7* is downregulated in lung cancer and is therefore useful as a biomarker and potential therapeutic agent[45]. *Let-7a* and *let-7b* have two nucleotide differences (see the sequences in Supplementary Table S1), and their probes are P_a and P_b, respectively. The hybrids *let-7a*·P_a and *let-7b*·P_b were fully matched, but

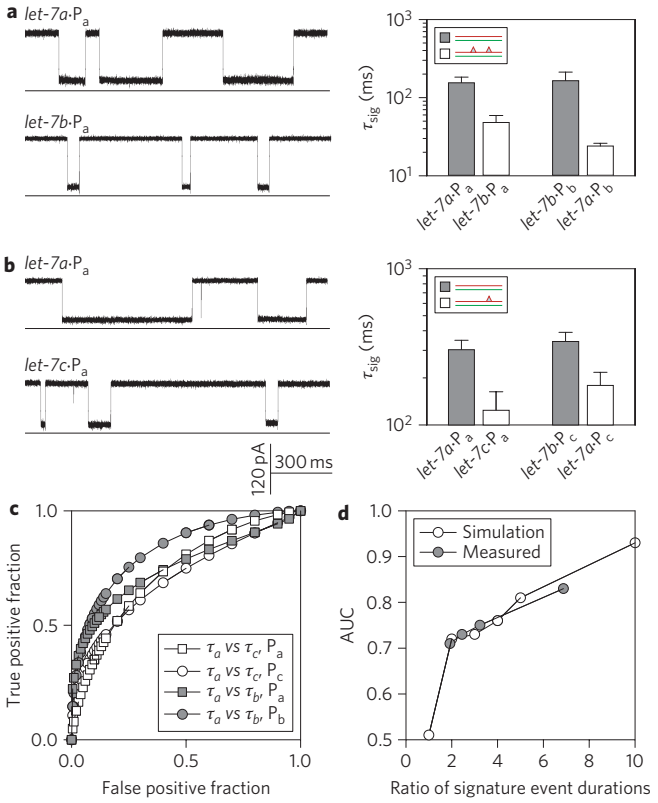

Figure 3 | Differentiation of *let-7* microRNAs that contain one or two different nucleotides. The sequences of *let-7a*, *let-7b* and *let-7c* are provided in Supplementary Table S1. **a**, Detection of *let-7a* and *let-7b* using the probe P_a or P_b at +120 mV. Left: current traces. Right: duration of signature events. **b**, Detection of *let-7a* and *let-7c* using the probe P_a or P_c at +100 mV. Left: current traces. Right: duration of signature events. See Supplementary Fig. S4 for a representative histogram and Supplementary Table S4 for raw data. **c**, ROC curves for the discrimination of events for fully matched microRNA·probe hybrids (defined as positive events) and microRNA·probe hybrids containing mismatched base pairs (defined as negative events). Open squares: *let-7a*·P_a/*let-7c*·P_a; open circles: *let-7c*·P_c/*let-7a*·P_c; filled squares: *let-7a*·P_a/*let-7b*·P_a; filled circles: *let-7b*·P_b/*let-7a*·P_b. **d**, Correlations between AUCs and the ratio of event duration for fully matched hybrids to those with mismatched base pairs. Filled circles: AUCs measured from the ROC curves in **c** (Supplementary Table S5); open circles: AUCs calculated from ROC analyses based on simulated data sets (Supplementary Fig. S5 and Table S6). The computer-generated event duration followed an exponential distribution. The ratios of event duration for ROC analysis were 1, 2, 3, 4, 5 and 10.

let-7b·P_a and *let-7a*·P_b contained two mismatches. The left panel of Fig. 3a shows the traces for *let-7a*·P_a and *let-7b*·P_a. The right panel shows that the unzipping time, τ_{sig}, at +120 mV for *let-7b*·P_a (48 ± 11 ms) is 3.2-fold shorter than that for *let-7a*·P_a (155 ± 28 ms) ($P < 0.005$), and 6.9-fold shorter when *let-7a*·P_b (24 ± 2 ms) is compared with *let-7b*·P_b (165 ± 47 ms) ($P < 0.005$). Similarly, *let-7a* and *let-7c* have only one nucleotide difference. The left panel of Fig. 3b shows the traces for *let-7a*·P_a and *let-7c*·P_a. The right panel shows that when using P_a and P_c to target *let-7a* and *let-7c* at +100 mV, respectively, τ_{sig} decreased by a factor of 2.4 from 303 ± 45 ms for *let-7a*·P_a to 124 ± 39 ms for *let-7c*·P_a ($P < 0.005$) and by a factor of 2.0 from 342 ± 49 ms for *let-7c*·P_c to 179 ± 38 ms for *let-7a*·P_c ($P < 0.005$).

We constructed receiver operating characteristic (ROC) curves to compare the durations of events for fully matched microRNA·probe hybrids and for microRNA·probe hybrids that contain mismatches (Fig. 3c). On the basis of ROC curves, we measured the area under the ROC curve (AUC, Fig. 3d), which is an indicator of the ability to discriminate nucleotide differences between microRNAs. The AUCs varied between 0.72 and 0.83, and increased with the ratio of event duration between fully matched hybrids and mismatches. The ratio-dependent AUC was further verified using a simulation method (Fig. 3d, Supplementary Fig. S5 and Supplementary Table S6). ROC analysis strongly suggests that the nanopore is able to discriminate SNPs in microRNAs based on the duration of the signature event. The ability to discriminate SNPs in the microRNAs was tested in a mixture of 100 nM *let-7a* and *let-7c* and probed with P_a. On the basis of the AUCs, the optimal cut-point duration was calculated to be ~190 ms, which was the threshold duration that provided the best discriminatory ability (Supplementary Table S6). Block events that were longer than the optimal cut-point occurred for *let-7a*·P_a, and events that were shorter than the optimal cut-point occurred for *let-7c*·P_a. The number of events was transformed into concentrations of *let-7a* and *let-7c*, which were 85 and 120 nM, respectively. Both concentrations varied by 15–20% from the real concentration of 100 nM.

Detection of microRNA levels in lung cancer patients

Lung cancer is the leading cause of cancer mortality in men and women worldwide and is responsible for about 1.2 million deaths each year[46]. Because no effective screening procedure is available, more than 70% of patients are diagnosed at advanced stages, with a five-year survival rate of less than 15% (ref. 46). At present, over one hundred microRNAs have been identified to be dysregulated in lung cancer[7–13,17,33,41]. High levels of miR-155 and low levels of *let-7a-2* correlate with significantly poor prognoses and shorter survival times in lung cancer patients[47,48].

We detected plasma miR-155 in lung cancer patients using the nanopore sensor. Peripheral blood samples were obtained from six lung cancer patients and six healthy volunteers after local Institutional Review Board approval. Total plasma RNAs, which contained microRNAs, were extracted from 350 μl of each plasma sample using a mirVana PARIS Kit (Ambion), with a final elution volume of 100 μl. The elution volumes were then divided into two 50 μl aliquots for the nanopore and qRT-PCR assays, respectively. One aliquot was mixed in the recording solution with or without the P_{155} probe. The nanopore current retained a low level of noise even in the presence of plasma extracts. In the absence of P_{155}, only short blocks were observed as a translocation of single-stranded oligonucleotides such as free microRNAs in the healthy individuals control group (Fig. 4a) and the lung cancer group (Fig. 4b). In the presence of the probe, distinct short and long blocks were identified in both the healthy individuals control group (Fig. 4c) and the lung cancer group (Fig. 4d). Characteristic long blocks shared the same current profile and properties as synthetic miR-155 RNA (Fig. 1). The frequency of long blocks in the lung cancer group was significantly higher than that in the healthy individuals group. More frequent short events were also observed in the presence of P_{155} (Fig. 4c,d) than without P_{155} (Fig. 4a, b). Most of these short events were contributed by the P_{155} probe, because its translocation rate was 8.4 times higher than that of microRNA (Supplementary Fig. S6). Overall, the characteristic long blocks were attributed to miR-155·P_{155} hybrids and served as signatures for the identification of single molecules of miR-155.

To normalize the assay, the frequencies of miR-155 signature events (f_{155}) for all the samples of the lung cancer and control groups were measured in the presence of a spiked-in synthetic *C. elegans* microRNA miR-39. Figure 4e shows that all the f_{155} values in the lung cancer group were higher than those in the control group ($P < 0.001$). However, Fig. 4f shows that the

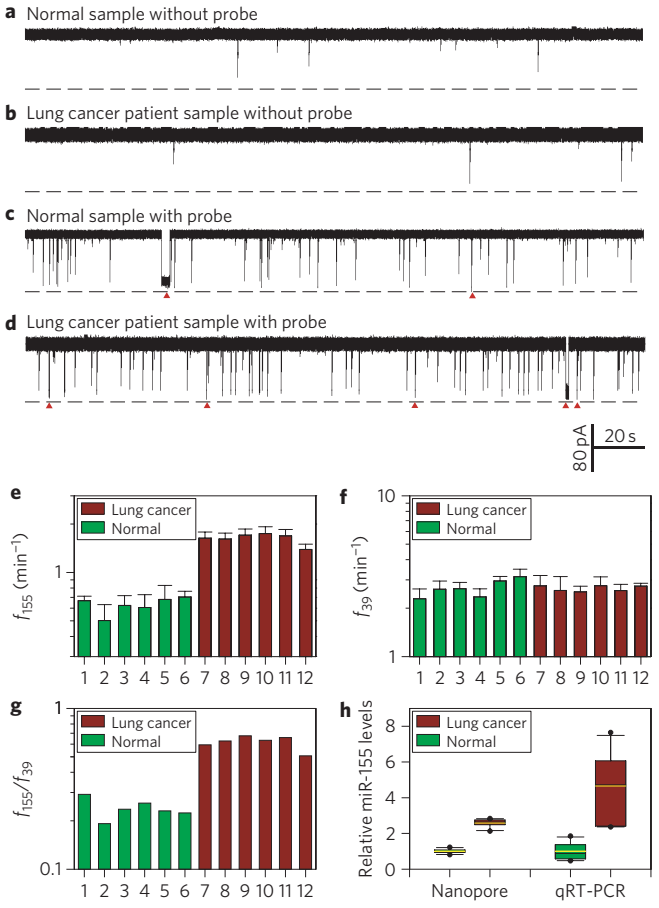

Figure 4 | Detection of miR-155 in the plasma of lung cancer patients. **a**–**d**, Current traces for total plasma RNAs from healthy volunteers (normal sample) and lung cancer patients without (**a**,**b**) and with (**c**,**d**) the P_{155} probe. Traces were recorded in 1 M KCl at +100 mV. Red arrows are signature events. Signature events were seen only in the presence of the 100 nM probe for both healthy volunteers (**c**) and lung cancer patients (**d**). **e**, Frequencies of miR-155 signature events (f_{155}) from six healthy individuals (1–6) and six patients with lung cancer (7–12) in the presence of spiked-in synthetic miR-39. **f**, Frequencies of miR-39 signature events detected using P_{39} (sequence in Supplementary Table S1) from all the samples that were used in **e**. Each sample was measured n times ($n \geq 4$) using independent nanopores. Data are mean ± s.d. Conditions of patients: 7, metastatic squamous lung carcinoma; 8, recurrent small-cell cancer; 9, early-stage small-cell carcinoma, status post-chemotherapy and radiation; 10, early-stage small-cell cancer, status post-chemotherapy; 11, late-stage non-small-cell carcinoma, status post-resection and post-chemotherapy; 12, late-stage adenocarcinoma, status post-chemotherapy. **g**, f_{155}/f_{39} calculated from panels **e** and **f**. **h**, Box and whisker plots of the relative miR-155 levels in healthy and lung cancer groups measured with the nanopore sensor and qRT-PCR. Boxes mark the intervals between the 25th and 75th percentiles. Black lines inside the boxes denote medians. Whiskers denote the intervals between the 5th and 95th percentiles. Filled circles indicate data points outside the 5th and 95th percentiles (see Supplementary Table S7 for raw data).

frequencies of spiked-in miR-39 events (f_{39}) were independent of the samples ($P > 0.05$). To evaluate the variability during total RNA extraction, the spiked-in miR-39 was used as an internal control and the ratio f_{155}/f_{39} was used to normalize the assays. Figure 4g shows that the mean f_{155}/f_{39} ratio in the lung cancer group (0.62 ± 0.06) was significantly higher than that in the control group (0.24 ± 0.05) ($P < 0.001$). The relative levels of miR-155 that were measured with the nanopore were also compared using the qRT-PCR method (Fig. 4h). Collectively, the mean level of miR-155 was increased by a factor of 2.6 in the lung cancer group compared with the control group as measured by the nanopore sensor ($P < 0.001$), but a 4.3-fold increase was obtained using the qRT-PCR method ($P < 0.02$). In addition, greater variability was observed in the qRT-PCR assay. Therefore, although both the nanopore and qRT-PCR assays indicated a significant increase of miR-155 in lung cancer patient samples, the nanopore method demonstrated higher accuracy with no requirement for labelling or amplification (Fig. 4h).

Conclusion

We have designed a nanopore-based microRNA sensor that uses a programmable oligonucleotide probe to generate a signature electrical signal for the direct and label-free detection of target microRNA in a fluctuating background, such as plasma RNA extracts from clinical samples. The key component of the nanopore sensor is the probe, the sequence of which is programmable and can be optimized to achieve high sensitivity and selectivity. We expect that the probe composition will not be limited to the four nucleotides. The incorporation of unnatural compounds such as locked nucleic acids and peptide nucleotide acids into the probe sequences may enhance selectivity because of the strengthened hybridization between probe and target. The probe can also be engineered with a specific barcode through chemical modification[31,49], so that multiple microRNAs can be simultaneously detected using distinct probes. Our sensor can detect microRNAs, various nucleic acid fragments, genetic alterations and pathogenic DNAs/RNAs. In the future, our nanopore sensor can be devised on new membrane platforms such as a droplet–interface bilayer[50] to construct stable nanopore arrays for high-throughput microRNA detection. Overall, the nanopore method can be a useful tool for quantitative studies of microRNAs and the discovery of disease markers, which are important for non-invasive screening and the early diagnosis of diseases such as cancer.

Materials and methods

Oligonucleotides, including microRNAs and DNA probes, were synthesized and electrophoresis-purified by Integrated DNA Technologies. Before testing, the mixture of each microRNA and the probe were heated to 90 °C for 5 min, gradually cooled to room temperature and stored at 4 °C. RNase-free water was used to prepare RNA samples.

Nanopore electrical recording. The nanopore detection method has been well documented[29,42]. The lipid bilayer membrane of 1,2-diphytanoyl-*sn*-glycerophosphatidylcholine (Avanti Polar Lipids) was formed spanning a 100–150 nm hole in the centre of a Teflon film that partitioned two chambers (*cis* and *trans*). The recording solutions on each side of the bilayer contained KCl at a desired concentration and were buffered with 10 mM Tris (pH 8.0). The α-haemolysin protein was inserted into the bilayer to form a pore from the *cis* side. MicroRNAs, DNA probes and plasma RNA extracts were also added to the *cis* solution. The voltage was given from the *trans* solution and the *cis* solution was grounded, so that a positive voltage could drive the translocation of a negatively charged DNA through the pore from *cis* to *trans*. Nanopore currents were recorded with an Axopatch 200A amplifier (Molecular Devices), filtered with a built-in four-pole low-pass Bessel filter at 5 kHz and acquired with Clampex 9.0 software (Molecular Devices) through a Digidata 1332 analog-to-digital converter (Molecular Devices) at a sampling rate of 20 kHz. Data were analysed using Clampfit 9.0 (Molecular Devices), Excel (MicroSoft) and SigmaPlot (SPSS) software. Because the signature events for the microRNA·probe ($\sim 10^1$–10^3 ms) were well separated from the oligonucleotide translocation events ($\sim 10^1$–10^2 μs) in duration, we set 1 ms as the boundary to collect each type of event. Data were presented as mean ± s.d. of three independent experiments, and the differences were considered statistically significant at $P < 0.05$ using the Student's *t*-test. Nanopore measurements were conducted at 22 ± 2 °C.

Total RNA extraction from plasma. Peripheral blood samples were obtained from the University of Missouri Ellis Fischel Cancer Center with Institutional Review Board approval. Whole blood with EDTA preservative was centrifuged at 1,600*g* for 10 min at room temperature and the plasma was transferred to new tubes. Total RNAs containing microRNAs were extracted from 350 μl of plasma using the

mirVana PARIS Kit (Ambion) according to the manufacturer's protocol. The final elution volume was 100 μl.

MicroRNA quantification by qRT-PCR. A SYBR Green-based qRT-PCR assay was used for microRNA quantification. About 10 μl of total RNA sample containing microRNAs was polyadenylated by poly(A) polymerase (Ambion) and reverse transcribed to cDNA using SuperScript III Reverse Transcriptase (Invitrogen) according to the manufacturer's instructions with a poly(T) adapter primer (5′-GCGAGCACAGAATTAATACGACTCACTATAGGTTTTTTTTTTTTTTVN-3′). Real-time PCR was performed using iQ SYBR Green Supermix (Bio-Rad) with the miR-155 specific forward primer (5′-TTAATGCTAATCGTGATAGGGGT-3′) and the sequence complementary to the poly(T) adapter as the reverse primer (5′-GCGAGCACAGAATTAATACGAC-3′) in an iQ5 Real-time PCR system (Bio-Rad). PCR was carried out at an initial denaturation at 95 °C for 3 min, followed by 40 cycles of 95 °C for 15 s and 60 °C for 1 min. The relative level of miR–155 was calculated using the $2^{-\text{delta Ct}}$ method, where the level of normal plasma was normalized as 1.

Normalization of the nanopore and qRT-PCR data using spiked-in *C. elegans* microRNA miR-39 as control. We introduced spiked-in synthetic microRNA as control to validate the nanopore sensor's capability of detecting microRNA in human samples. The spiked-in RNA oligonucleotide in the detection matches the sequence of *C. elegans* miR-39, a microRNA that is absent in the human genome. About 3.5 μl of 1 nM synthetic miR-39 solution was introduced to each 350 μl plasma sample after the addition of 2× denaturing solution (mirVana PARIS Kit) to plasma; thus the miR-39 concentration in plasma was 10 pM. The denaturing solution prevents RNAs from degradation by inhibiting endogenous plasma RNases. For each sample, both miR-155 and spiked-in miR-39 were measured using the nanopore sensor and SYBR Green-based qRT-PCR. Nanopore data and the normalization result are shown in Supplementary Table S7. In nanopore detection, the probes for miR-155 and miR-39 were P_{155} and P_{39}. We first measured the signature event frequencies, f_{155} and f_{39}, of hybrids miR-155·P_{155} and miR-39·P_{39}, respectively. The variability of f_{39} reflecs the difference in miR-39 concentrations among samples after RNA extraction. Therefore, the ratio of the two frequencies, f_{155}/f_{39}, should eliminate this variability. Finally, the mean f_{155}/f_{39} ratio of six normal samples (A_{normal}) was used as the standard to calculate each sample's relative miR-155 level by normalizing f_{155}/f_{39} to A_{normal}, that is, $f_{155}/f_{39}/A_{\text{normal}}$.

Received 26 April 2011; accepted 29 July 2011; published online 4 September 2011

References

1. Carthew, R. W. & Sontheimer, E. J. Origins and mechanisms of miRNAs and siRNAs. *Cell* **136,** 642–655 (2009).
2. Inui, M., Martello, G. & Piccolo, S. MicroRNA control of signal transduction. *Nature Rev. Mol. Cell Biol.* **11,** 252–263 (2010).
3. Lee, R. C., Feinbaum, R. L. & Ambros, V. The *C. elegans* heterochronic gene *lin-4* encodes small RNAs with antisense complementarity to *lin-14*. *Cell* **75,** 843–854 (1993).
4. Kozomara, A. & Griffiths-Jones, S. miRBase: integrating microRNA annotation and deep-sequencing data. *Nucleic Acids Res.* **39,** D152–D157 (2011).
5. Bartel, D. P. MicroRNAs: genomics, biogenesis, mechanism, and function. *Cell* **116,** 281–297 (2004).
6. Diederichs, S. & Haber, D. A. Dual role for argonautes in MicroRNA processing and posttranscriptional regulation of MicroRNA expression. *Cell* **131,** 1097–1108 (2007).
7. Garzon, R., Calin, G. A. & Croce, C. M. MicroRNAs in cancer. *Ann. Rev. Med.* **60,** 167–179 (2009).
8. Ortholan, C. *et al.* MicroRNAs and lung cancer: new oncogenes and tumor suppressors, new prognostic factors and potential therapeutic targets. *Curr. Med. Chem.* **16,** 1047–1061 (2009).
9. Calin, G. A. & Croce, C. M. MicroRNA signatures in human cancers. *Nature Rev. Cancer* **6,** 857–866 (2006).
10. Mitchell, P. S. *et al.* Circulating microRNAs as stable blood-based markers for cancer detection. *Proc. Natl Acad. Sci. USA* **105,** 10513–10518 (2008).
11. Kosaka, N. *et al.* Secretory mechanisms and intercellular transfer of microRNAs in living cells. *J. Biol. Chem.* **285,** 17442–17452 (2010).
12. Rabinowits, G., Gerçel-Taylor, C., Day, J. M., Taylor, D. D. & Kloecker, G. H. Exosomal microRNA: a diagnostic marker for lung cancer. *Clin. Lung Cancer* **10,** 42–46 (2009).
13. Rosell, R., Wei, J. & Taron, M. Circulating MicroRNA signatures of tumor-derived exosomes for early diagnosis of non-small-cell lung cancer. *Clin. Lung Cancer* **10,** 8–9 (2009).
14. Chen, C. *et al.* Real-time quantification of microRNAs by stem-loop RT-PCR. *Nucleic Acids Res.* **33,** e179 (2005).
15. Li, W. & Ruan, K. MicroRNA detection by microarray. *Anal. Bioanal. Chem.* **394,** 1117–1124 (2009).
16. Hunt, E. A., Goulding, A. M. & Deo, S. K. Direct detection and quantification of microRNAs. *Anal. Biochem.* **387,** 1–12 (2009).
17. Yendamuri, S. & Kratzke, R. MicroRNA biomarkers in lung cancer: MiRacle or quagMiRe? *Transl. Res.* **157,** 209–215 (2011).
18. Neely, L. A. *et al.* A single-molecule method for the quantitation of microRNA gene expression. *Nature Methods* **3,** 41–46 (2006).
19. Bayley, H. & Jayasinghe, L. Functional engineered channels and pores — (Review). *Mol. Membrane Biol.* **21,** 209–220 (2004).
20. Gu, L. Q. & Shim, J. W. Single molecule sensing by nanopores and nanopore devices. *Analyst* **135,** 441–451 (2010).
21. Howorka, S. & Siwy, Z. Nanopore analytics: sensing of single molecules. *Chem. Soc. Rev.* **38,** 2360–2384 (2009).
22. Ma, L. & Cockroft, S. L. Biological nanopores for single-molecule biophysics. *Chembiochem* **11,** 25–34 (2010).
23. Movileanu, L. Interrogating single proteins through nanopores: challenges and opportunities. *Trends Biotechnol.* **27,** 333–341 (2009).
24. Olasagasti, F. *et al.* Replication of individual DNA molecules under electronic control using a protein nanopore. *Nature Nanotech.* **5,** 798–806 (2010).
25. Bayley, H. Sequencing single molecules of DNA. *Current Opin. Chem. Biol.* **10,** 628–637 (2006).
26. Branton, D. *et al.* The potential and challenges of nanopore sequencing. *Nature Biotechnol.* **26,** 1146–1153 (2008).
27. Wanunu, M. *et al.* Rapid electronic detection of probe-specific microRNAs using thin nanopore sensors. *Natur Nanotech.* **5,** 807–814 (2010).
28. Song, L. Z. *et al.* Structure of staphylococcal alpha-hemolysin, a heptameric transmembrane pore. *Science* **274,** 1859–1866 (1996).
29. Kasianowicz, J. J., Brandin, E., Branton, D. & Deamer, D. W. Characterization of individual polynucleotide molecules using a membrane channel. *Proc. Natl Acad. Sci. USA* **93,** 13770–13773 (1996).
30. Meller, A., Nivon, L. & Branton, D. Voltage-driven DNA translocations through a nanopore. *Phys. Rev. Lett.* **86,** 3435–3438 (2001).
31. Mitchell, N. & Howorka, S. Chemical tags facilitate the sensing of individual DNA strands with nanopores. *Angew. Chem. Int. Ed.* **47,** 5565–5568 (2008).
32. Meller, A., Nivon, L., Brandin, E., Golovchenko, J. & Branton, D. Rapid nanopore discrimination between single polynucleotide molecules. *Proc. Natl Acad. Sci. USA* **97,** 1079–1084 (2000).
33. Donnem, T. *et al.* Prognostic impact of miR-155 in non-small cell lung cancer evaluated by in situ hybridization. *J. Transl. Med.* **9,** 6 (2011).
34. Mathé, J., Visram, H., Viasnoff, V., Rabin, Y. & Meller, A. Nanopore unzipping of individual DNA hairpin molecules. *Biophys. J.* **87,** 3205–3212 (2004).
35. Sauer-Budge, A. F., Nyamwanda, J. A., Lubensky, D. K. & Branton, D. Unzipping kinetics of double-stranded DNA in a nanopore. *Phys. Rev. Lett.* **90,** 238101 (2003).
36. Butler, T. Z., Gundlach, J. H. & Troll, M. Ionic current blockades from DNA and RNA molecules in the alpha-hemolysin nanopore. *Biophys. J.* **93,** 3229–3240 (2007).
37. Mathé, J., Aksimentiev, A., Nelson, D. R., Schulten, K. & Meller, A. Orientation discrimination of single-stranded DNA inside the alpha-hemolysin membrane channel. *Proc. Natl Acad. Sci. USA* **102,** 12377–12382 (2005).
38. Purnell, R. F., Mehta, K. K. & Schmidt, J. J. Nucleotide identification and orientation discrimination of DNA homopolymers immobilized in a protein nanopore. *Nano. Lett.* **8,** 3029–3034 (2008).
39. Wanunu, M., Morrison, W., Rabin, Y., Grosberg, A. Y. & Meller, A. Electrostatic focusing of unlabelled DNA into nanoscale pores using a salt gradient. *Nature Nanotech.* **5,** 160–165 (2010).
40. Maglia, G., Restrepo, M. R., Mikhailova, E. & Bayley, H. Enhanced translocation of single DNA molecules through α-hemolysin nanopores by manipulation of internal charge. *Proc. Natl. Acad. Sci. USA* **105,** 19720–19725 (2008).
41. Cho, W. C. Role of miRNAs in lung cancer. *Expert Rev. Mol. Diagn.* **9,** 773–776 (2009).
42. Howorka, S., Cheley, S. & Bayley, H. Sequence-specific detection of individual DNA strands using engineered nanopores. *Nature Biotechnol.* **19,** 636–639 (2001).
43. Nakane, J., Wiggin, M. & Marziali, A. A nanosensor for transmembrane capture and identification of single nucleic acid molecules. *Biophys. J.* **87,** 615–621 (2004).
44. Vercoutere, W. *et al.* Rapid discrimination among individual DNA hairpin molecules at single-nucleotide resolution using an ion channel. *Nature Biotechnol.* **19,** 248–252 (2001).
45. Landi, M. T. *et al.* MicroRNA expression differentiates histology and predicts survival of lung cancer. *Clin. Cancer Res.* **16,** 430–441 (2010).
46. Silvestri, G. A., Alberg, A. J. & Ravenel, J. The changing epidemiology of lung cancer with a focus on screening. *Br. Med. J.* **339,** 63053 (2009).
47. Patnaik, S. K., Kannisto, E., Knudsen, S. & Yendamuri, S. Evaluation of microRNA expression profiles that may predict recurrence of localized stage I non-small cell lung cancer after surgical resection. *Cancer Res.* **70,** 36–45 (2010).
48. Yanaihara, N. *et al.* Unique microRNA molecular profiles in lung cancer diagnosis and prognosis. *Cancer Cell* **9,** 189–198 (2006).
49. Singer, A. *et al.* Nanopore based sequence specific detection of duplex DNA for genomic profiling. *Nano Lett.* **10,** 738–742 (2010).
50. Bayley, H. *et al.* Droplet interface bilayers. *Mol. Biosyst.* **4,** 1191–1208 (2008).

Acknowledgements

The authors thank K. Gillis, T-C. Hwang, S-J. Chen, F. Hsieh and M. Milanick for invaluable discussions on experimental design and data analysis. This investigation was partially supported by grants from the National Science Foundation 0546165 (L-Q.G.), the National Institutes of Health GM079613 (L-Q.G.) and the University of Missouri Intellectual Property Fast Track Initiative (A8881, M.X.W.), and was conducted in a facility that was constructed with support from the Research Facilities Improvement Program grant no. C06-RR-016489-01 from the National Centre for Research Resources, National Institutes of Health.

Author contributions

Y.W. designed and performed the nanopore experiments, collected and analysed the nanopore data, and co-wrote the manuscript. D.Z. designed and performed the qRT-PCR experiments, analysed the qRT-PCR data and co-wrote the manuscript. Q.T. performed molecular biology experiments, including protein synthesis. M.X.W. conceived the qRT-PCR experiments, provided the patients' samples and co-wrote the manuscript. L-Q.G. conceived the principal idea, designed the nanopore experiments and wrote the manuscript. All the authors discussed the results and commented on the manuscript.

Additional information

The authors declare no competing financial interests. Supplementary information accompanies this paper at www.nature.com/naturenanotechnology. Reprints and permission information is available online at http://www.nature.com/reprints. Correspondence and requests for materials should be addressed to M.X.W. and L-Q.G.